Radiological Physics and Technology (2019) 12:137–148
https://doi.org/10.1007/s12194-019-00502-0

Comparison of volumetric-modulated arc therapy and intensity-modulated radiation therapy prostate cancer plans accounting for cold spots

Tran Thi Thao Nguyen[1,4] · Hidetaka Arimura[2] · Ryosuke Asamura[1] · Taka-aki Hirose[1,3] · Saiji Ohga[2] · Jun-ichi Fukunaga[3]

Received: 8 July 2018 / Revised: 7 February 2019 / Accepted: 11 February 2019 / Published online: 25 February 2019

Abstract
This study compared dosimetric indices of volumetric-modulated arc therapy (VMAT) with intensity-modulated radiation therapy (IMRT) accounting for cold spots in prostate cancer plans. IMRT plans were retrospectively generated from 30 prostate cancer patients with ten cases for each risk group, who received VMAT plans. The mean, maximum, and minimum doses, and conformity and homogeneity indexes were evaluated for planning target volume (PTV) and the mean dose and *V*20–*V*70 for organs at risk (OAR) including the rectum, bladder, right and left femoral heads, and rectum overlapped with PTV (ROP) regions. The numbers and volume percentages of cold spots within PTVs and ROP regions were measured using in-house software. Three-dimensional probabilistic distributions of the probability and distributions of cold spots were generated using a centroid matching technique for visualization and analysis. There was a statistically better dose conformity in the PTV, rectum, and bladder dose-sparing in VMAT compared to that in the IMRT plans, whereas VMAT had statistically worse target dose homogeneity, and right and left femoral head dose-sparing than those of the IMRT plans. The average volume percentage of cold spots per PTV for the VMAT was $4.37 \pm 2.68\%$, which was smaller than the $5.72 \pm 1.84\%$ observed for IMRT plans ($P = 0.007$). The volume percentage of cold spots per ROP for the VMAT did not significantly differ from those for the IMRT plans. Compared with IMRT, the VMAT plans achieved better PTV dose conformity, OAR dose-sparing, and smaller cold spots in the treatment of prostate cancer.

Keywords Prostate cancer · Cold spot · VMAT · IMRT · Probabilistic distribution

1 Introduction

Recently, prostate cancer is one of the most common malignant diseases in men worldwide, especially those in developed countries [1]. Prostate cancer is the seventh leading cause of cancer death in Japanese men [2]. In general, the treatment options for prostate cancer include prostatectomy, chemotherapy, hormonotherapy, and radiotherapy. There has been a significant increase in the number of prostate cancer patients treated with volumetric-modulated arc therapy (VMAT) and intensity-modulated radiation therapy (IMRT) in Japan [3] because of their lower risks of urinary and sexual dysfunctions. In static IMRT (step-and-shoot technique), a multileaf collimator (MLC) divides each radiation beam into a set of smaller segments of differing MLC shape to conform to and administer high doses to the tumor and improve sparing of normal tissue and organs at risk (OAR), resulting in the reduction of acute and late toxicities [4, 5].

✉ Hidetaka Arimura
arimurah@med.kyushu-u.ac.jp

1 Division of Medical Quantum Science, Department of Health Sciences, Graduate School of Medical Sciences, Kyushu University, 3-1-1, Maidashi, Higashi-ku, Fukuoka 812-8582, Japan

2 Division of Medical Quantum Science, Department of Health Sciences, Faculty of Medical Sciences, Kyushu University, 3-1-1, Maidashi, Higashi-ku, Fukuoka 812-8582, Japan

3 Department of Medical Technology, Kyushu University Hospital, 3-1-1, Maidashi, Higashi-ku, Fukuoka 812-8582, Japan

4 Japan Society for the Promotion of Science, 5-3-1, Kojimachi, Chiyoda-ku, Tokyo 102-0083, Japan

In dynamic IMRT (sliding window technique), multiple fixed angle radiation beams and continuously moving MLC are used to modulate the intensity of each radiation beam [6, 7]. VMAT delivers radiation doses while varying the MLC motion, dose rate, and gantry rotation speed [8].

However, in VMAT and IMRT treatment plans, there are trade-offs in target coverage and OAR dose-sparing, which result in routine encountering of high-dose (hot spots) and low-dose (cold spots) regions in the planning target volume (PTV) [9–12]. According to the study of Tomé et al. on the effect of a small volume of cold spots on TCP for solid tumors, one of the causes of tumor recurrences is the occurrence of cold spots in target volume because cold spots could lead to the decrease of TCP [13]. To focus on the tumor control, we deal only with cold spots in this study.

In general, cold spots are defined as volumes of tissue that receive doses less than an applicable percentage of the prescribed dose [10]. We should use the definition of the cold spots for prostate cancer plans. However, to the best of our knowledge, at present there is no generally acceptable consensus regarding the magnitude, volume, and distribution for cold spots for most of cancer types, including prostate cancer. Therefore, we employed the trial guidelines of the Radiation Therapy Oncology Group (RTOG) H-0222 [10] for this study, which provided recommendations, including cold spots, for head and neck cancer. The cold spots are defined as regions that receive doses lower than 93% of the prescribed dose within PTV [10]. The total volume of cold spots should be $< 1\%$ of the PTV [10]. The locations of cold spots are important, because they should not be located within the gross tumor volume (GTV) and ideally should be at the periphery of the PTV, as far as from the GTV as possible [10]. Therefore, it is essential to understand the distributions of the probability of the existence of cold spots and the distributions of the cold spots if they were to occur in radiation therapy plans. Several studies have shown that underdosing even small fractions of the target volume can result in a reduction of tumor control probability (TCP), which would cause recurrences of tumors due to insufficient irradiation to PTV [12–15]. Vora et al. evaluated the long-term control of the disease and chronic toxicities observed in patients treated with IMRT for prostate cancer [14]. The results of their study showed that local and distant recurrent rates of 5% and 8.6%, respectively. In addition, the 9-year biochemical control rates were 77.4% for low-risk patients, 69.6% for intermediate-risk patients, and 53.3% for high-risk patients who received IMRT [14].

Several reports on VMAT and IMRT plans have been published [16–25]. Wolff et al. reported that both VMAT and IMRT yielded treatment plans of improved quality in comparison with three-dimensional (3D) conformal treatments, by analyzing their dose distributions with various dosimetric indices [17]. Quan et al. evaluated the differences in plan qualities between VMAT and IMRT while considering the delivery time and the number of beams in IMRT [18]. However, to the best of our knowledge, no studies have compared VMAT and IMRT plans with respect to not only target dose conformity and homogeneity, rectum overlapped with PTV (ROP) [26] dose-sparing and OAR (rectum, bladder, right and left femoral heads) dose-sparing but also the number, volume, and probabilistic distributions (PD) of cold spots in the PTV and ROP region in the treatment of prostate cancer.

Therefore, the aim of this study was to compare VMAT with IMRT, accounting for cold spots in prostate cancer plans. In this study, the mean, maximum, and minimum doses, and conformity and homogeneity indexes were evaluated for the PTV; the mean dose and $V20$–$V70$ for OAR including the rectum, bladder, right and left femoral heads, and ROP regions. Cold spots in the ROP regions may be associated with recurrences of tumors. Therefore, in this study, we investigated the cold spots in the ROP regions to understand how the magnitude, volume, and distribution of these low-dose regions are different in the ROP regions between the VMAT and IMRT plans. In addition, the numbers and volume percentages of cold spots within PTVs and ROP regions were measured using in-house software. 3D PD of the probability and distributions of cold spots were generated using a centroid matching technique for their visualization and analysis.

2 Materials and methods

2.1 Clinical cases

This study was performed under the approval of the institutional review board of our hospital. Thirty patients (median age 72 years; range 56–87 years; stage T1–T3a) treated with VMAT for prostate cancer were selected for this study. These cases included ten low-risk patients, ten intermediate-risk patients, and ten high-risk patients. The reason for using three risk categories is that the magnitude, volume, and distribution of cold spots within the PTVs may depend on the contours of three risk clinical target volumes (CTVs). The low-, intermediate-, and high-risk CTVs were defined as containing only the prostate, prostate plus 1-cm proximal seminal vesicles, and prostate plus 2-cm proximal seminal vesicles, respectively [27, 28]. PTV margins (internal and set-up margins) were added as 5 mm in posterior direction to spare additional rectal tissue from receiving radiation dose and 8 mm in other directions. The median volumes of the PTVs with its range were 101.62 cc (52.35–132.73 cc) for the low-risk group, 106.87 cc (75.99–159.25 cc) for the intermediate-risk group, 97.45 cc (75.59–137.63 cc) for the high-risk group, and 103.78 cc (52.35–159.25 cc) for all-risk groups. The volumes (means $\pm$ SDs) of the PTVs were

96.22 ± 22.98 cc for the low-risk group, 111.85 ± 22.42 cc for the intermediate-risk group, 100.44 ± 21.18 cc for the high-risk group, and 102.44 ± 23.16 cc for all-risk groups.

IMRT plans were retrospectively generated from the 30 prostate cancer patients in three risk groups who received VMAT plans with a prescribed dose of 76 Gy in 38 fractions. The dose calculations for both techniques utilized an anisotropic analytical algorithm (AAA) [29], with a dose calculation grid size of 2.5 mm and 10-MV photon beam, which was the algorithm implemented in the Varian Eclipse, version 10.0, treatment planning system. In plans for both VMAT and IMRT in our hospital, the mean dose within the PTV was set as 100% of the prescribed dose [30]. For the rectum, 65, 70, and 76 Gy covered less than 25%, 20%, and 3% of the volume, respectively. For the bladder, 40 and 70 Gy covered less than 60% and 35% of the volume, respectively. For the ROP, the average dose ranged from 90 to 95% of the prescribed dose. For the right and left femoral heads, the maximum dose was less than 50 Gy. Dose criteria in our institute follow the RTOG 0126 guideline [30]. However, the OAR dose criteria were set as threshold values lower than these of RTOG 0126 due to a concern of reducing toxicity to OAR. Optimization parameters and their weightings (priorities) for VMAT and IMRT plans are summarized in Table 1.

The VMAT plans consisted of a single arc starting at a gantry angle of 179° and stopping at a gantry angle of 181° in the counter-clockwise direction [Varian International Electrotechnical Commission (IEC) scale]. The collimator was set to 30°. From the VMAT optimization, a series of MLC segments for each arc field was generated. One MLC segment formed an aperture shape from a beam at every two gantry positions, which translated to 178 segments for one full arc. The IMRT plans consisted of seven coplanar fields modulated with dynamic-MLC at gantry angles of 0°, 51°, 102°, 204°, 255°, and 306°. Leaf sizes of both MLCs for VMAT and IMRT were 5 mm. The gantry angles of the beams were manually selected based on the morphologic relationships between the PTVs and the OAR.

Table 1 Optimization parameters and their weightings (priorities) for VMAT and IMRT plans

Structure	Volume (%)	Dose (Gy)	Priority
CTV	100	76	90–98
Rectum_O	0	36–38	30–90
	30	20	40–65
	70	10	50
ROP	0	69–73	30–60
	100	68–70	50–80
PTV_Rectum	0	74–78	80–100
	100	75–77	70–100
Bladder	30	40	50
Rectum	0	68–70	50–80
Large bowel	0	45–60	60
	40	25	50

CTV clinical target volume, *PTV* planning target volume, *Rectum_O* rectum minus PTV with an extra 5-mm margin, *PTV_Rectum* PTV minus rectum, *ROP* rectum overlapped with PTV

We employed different optimization algorithms, i.e., the progressive resolution optimizer (PRO) algorithm for the VMAT plans and dose-volume optimizer (DVO) algorithm for the IMRT plans. The PRO algorithm creates the VMAT plans based on dose-volume objectives, and generates a sequence of control points, which define MLC leaf positions and MU/degree as a function of gantry angle. A multi-resolution approach (i.e. simulated annealing method [8]) and an objective function (the sum of the dose-volume and user-defined objectives) are used to optimize the VMAT plans. The DVO algorithm determines the optimal field shape and intensity by iteratively conforming the dose distribution to the desired objectives until an optimum solution is reached using simple gradient optimization.

A four-slice computed tomography (CT) scanner (Mx 8000; Philips, Amsterdam, The Netherlands) was used to acquire planning CT images with dimensions of 512 × 512 pixels, an in-plane pixel size of 0.977 mm, and a slice thickness of 2.0 mm. Figure 1 illustrates the contours of CTV, PTV, rectum, bladder, right femoral head, and left femoral head in an axial view for a low-risk prostate cancer patient. The rectum contours were delineated by inferiorly starting from the anorectal junction and superiorly extending up to the beginning of the sigmoid at the rectosigmoid junction. The bladder contours were delineated from its base to the dome. The femoral heads contours were delineated to the ball of the femur. The contours of the CTVs, PTVs and OAR were delineated on the planning CT images for each patient based on the consensus between a radiation oncologist (S.O.) and a medical physicist (T.H.) using a commercial radiation treatment planning (RTP) system. The dose distribution images had an in-plane pixel size of 2.5 mm and a slice thickness of 2.0 mm. The voxel size of the original dose distribution data (2.5 mm × 2.5 mm × 2.0 mm) differed from that of the PTV regions on the planning CT images (0.977 mm × 0.977 mm × 2.000 mm). Therefore, nearest-neighbor interpolation and linear interpolation methods were used on the PTV regions and dose distribution data, respectively, so that the isovoxel size (0.977 mm) of the PTV regions was equal to that of the dose distribution data [31].

2.2 Plan evaluation

The following dosimetric indices were evaluated based on the dose-volume histograms of the VMAT and IMRT plans: mean dose, maximum and minimum doses, conformity index (CI), homogeneity index (HI) for PTV, and the mean dose and

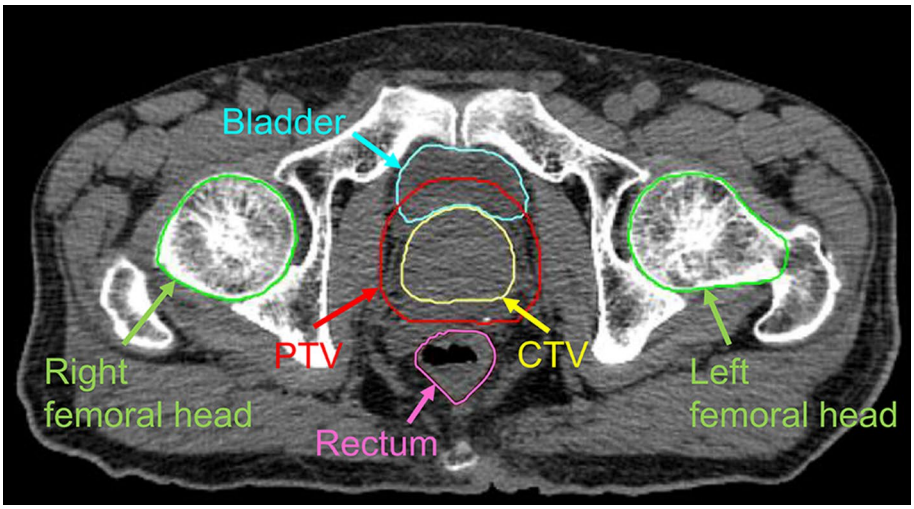

Fig. 1 An illustration of the contours of CTV, PTV, rectum, bladder, right femoral head, and left femoral head in an axial view for a low-risk prostate cancer patient

*V*20–*V*70 for OAR including the rectum, bladder, right and left femoral heads, and ROP regions.

The PTV doses were evaluated for the average, minimum, and maximum doses. To quantitatively evaluate dose the conformity and homogeneity in the PTV, the CI and HI were calculated [6, 32–34]. The CI was defined as

$$\mathrm{CI} = \frac{\mathrm{TV_{Dp}}}{V_{\mathrm{PTV}}} \times \frac{\mathrm{TV_{Dp}}}{V_{\mathrm{D_p}}}, \tag{1}$$

where $\mathrm{TV_{Dp}}$ was the PTV covered by the prescribed dose (cm^3), V_{PTV} the PTV (cm^3), and $V_{\mathrm{D_p}}$ was the volume of the prescribed dose (cm^3). The HI in the International Commission on Radiation Units and Measurements (ICRU) Report 83 is defined as

$$\mathrm{HI} = \frac{D_2 - D_{98}}{D_{50}}, \tag{2}$$

where D_2, D_{98}, and D_{50} were the minimum dose delivered to 2%, 98%, and 50% of the PTV. An HI value closer to 0 indicates a more homogeneous dose distribution within the PTV. The conformity index is a measure of how well the volume of the prescribed dose conforms to the size and shape of the PTV. A CI value closer to 1 indicates that the volume of the prescribed dose more closely conforms to the PTV.

Vx ($x = 20, 30, 40, 50, 60, 70$) was defined as the percentage of OAR (rectum, bladder, right and left femoral heads, and ROP regions) volume receiving x Gy and was used to represent the high-dose OAR volume.

2.3 Analysis of cold spots in the dose distributions

Figure 2 shows the overall scheme for the detection of cold spots in dose distributions. First, PTV regions were constructed from contours (DICOM structure data) on planning CT images. Second, the dose distributions within PTVs and ROP regions were extracted from the total dose distributions. Third, cold spot regions were detected by thresholding

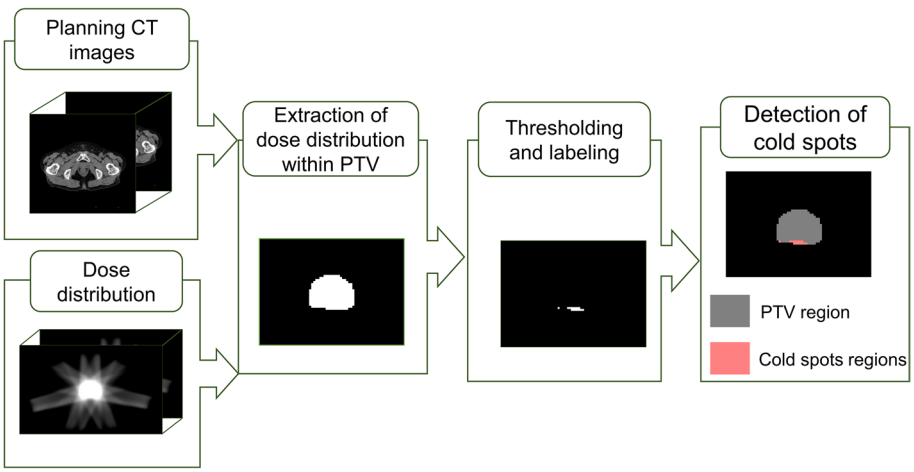

Fig. 2 An overall scheme for the detection of cold spots in dose distributions

the dose distributions within PTV regions according to the cold spot definition of dose regions lower than 93% of the prescribed dose. Finally, the detected cold spot regions were labeled using 26 connecting labeling [35, 36]. The numbers and volumes of the labeled cold spot regions were then calculated. In addition, for comparison of the VMAT and IMRT plans, the numbers and volumes of the cold spots were normalized by the PTVs. We developed in-house software according to the algorithm described above.

2.4 3D PD of the probability and distributions of cold spots

Figure 3 illustrates an overall scheme developed as in-house software to generate the PD of the probability and distributions of cold spots. The PD of the probability and distributions of cold spots were constructed by registration of all PTV and detected cold spots to a reference PTV (a median PTV) using a centroid matching technique [37]. The PD ($P(\boldsymbol{x}_i)$) of the probability and distributions of cold spots was calculated as

$$P(\boldsymbol{x}_i) = \frac{1}{N}\sum_{n=1}^{N} f_n(\boldsymbol{x}_i), \tag{3}$$

where $\boldsymbol{x}_i$ was the 3D coordinate of ith voxel, n the case number, N the number of cases, and $f_n(\boldsymbol{x}_i)$ was the ith voxel value (one or zero) of cold spots regions for a nth case.

Furthermore, we investigated the volumes of the cold-spot-existence PD by changing the probabilities. For 3D visualizations and analyses of the PD of the probability and distributions of cold spots, a red color with an opacity, which represented the degree of color transparency, was set to the value of the probability of the existence of cold spots ranging from 0 to 1. A logical OR indicates the mathematical operation in logic or the logical disjunction. The logical OR region of the PTVs is a set of voxels, in which the logical ORs are one after registering all PTVs to the reference PTV. Each PTV consists of a one-value voxel, but the outside voxels include a zero-value voxel. The logical OR region of the PTV was also visualized as a green color to analyze the location of cold spots in the PTV.

The visualization tool presented in this study can be used for verification of the presence or absence of cold spot regions in the CTV, because cold spots should not be located within the CTV but should be at the periphery of the PTV [10] according to RTOG H-0222.

2.5 Statistical analysis

To evaluate the differences between the VMAT and IMRT plans, statistical analysis was performed using two-sided paired Student's t tests. The difference was considered statistically significant for P values less than 0.05.

3 Results

Tables 2, 3, 4 and 5 show the averages and standard deviations of the dosimetric indices for the PTV, rectum, bladder, ROP, right femoral head, and left femoral head of the VMAT and IMRT plans for the low-risk group, the intermediate-risk group, the high-risk group, and all-risk groups, respectively. As for the PTV, there were no statistically significant differences in the CI and HI between VMAT and IMRT plans among the three risk groups (Tables 2, 3, 4). However, VMAT had statistically better dose conformity than that of the IMRT plans, whereas VMAT had statistically worse dose homogeneity than that of the IMRT plans for all-risk groups (Table 5).

For the rectum, the VMAT plans resulted in a lower average mean dose to the rectum and lower volume percentages of the rectum at every dose (20, 30, 40, 50, and 60 Gy) than those of the IMRT plans (Table 5). All differences between the VMAT and IMRT plans were statistically significant.

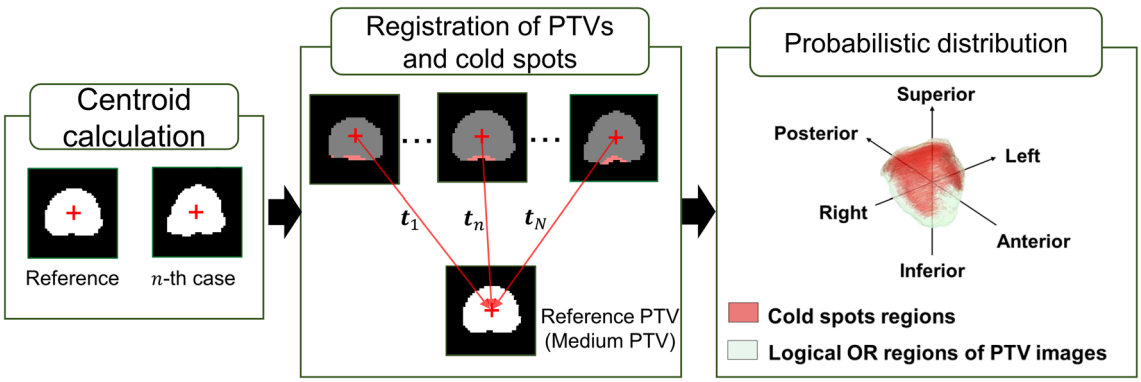

Fig. 3 An overall scheme for generating a probabilistic distribution of the probability and distributions of cold spots

Table 2 Averages and standard deviations of the dosimetric indices for PTV, rectum, bladder, ROP, right femoral head, and left femoral head of VMAT and IMRT plans for the low-risk group

	VMAT		IMRT		*P* value
	Average	±SD	Average	±SD	
PTV					
Mean dose (Gy)	76.00	0.00	76.00	0.00	–
Maximum dose (Gy)	79.51	0.65	78.13	0.36	**< 0.001**
Minimum dose (Gy)	61.37	2.37	62.19	2.36	0.111
CI	0.964	0.013	0.958	0.014	0.118
HI	0.103	0.022	0.096	0.021	0.344
Rectum					
Mean dose (Gy)	26.82	2.78	28.41	2.48	**< 0.001**
*V*20 (%)	53.71	4.28	58.81	5.17	**0.005**
*V*30 (%)	34.89	6.19	38.81	4.06	**0.007**
*V*40 (%)	23.35	5.60	25.46	4.92	**0.003**
*V*50 (%)	15.79	3.97	17.41	4.00	**< 0.001**
*V*60 (%)	10.03	2.59	11.16	2.62	**< 0.001**
*V*70 (%)	3.80	1.25	3.71	1.25	0.612
Bladder					
Mean dose (Gy)	26.29	11.61	27.29	11.59	**0.008**
*V*20 (%)	46.96	23.07	49.34	23.09	**0.004**
*V*30 (%)	38.04	21.54	40.26	21.58	**0.004**
*V*40 (%)	28.91	16.98	30.15	16.91	**0.017**
*V*50 (%)	21.67	12.27	22.76	12.53	**0.015**
*V*60 (%)	16.23	8.86	16.71	12.53	0.207
*V*70 (%)	10.15	5.96	10.76	5.52	**0.012**
ROP					
Mean dose (Gy)	69.89	1.01	69.92	1.19	0.890
*V*40 (%)	100.00	0.00	100.00	0.00	–
Right femoral head					
Mean dose (Gy)	15.35	2.96	14.03	2.73	0.217
*V*40 (%)	0.00	0.00	0.00	0.00	–
Left femoral head					
Mean dose (Gy)	16.12	1.55	13.89	2.73	**0.020**
*V*40 (%)	0.00	0.00	0.00	0.00	–

Values in bold are statistically significant

PTV planning target volume, *ROP* rectum overlapped with PTV, *VMAT* volumetric-modulated arc therapy, *IMRT* intensity-modulated radiation therapy, *SD* standard deviation, *CI* conformity index, *HI* homogeneity index, *Vx* percentage volume receiving at least *x* Gy

Table 3 Averages and standard deviations of the dosimetric indices for PTV, rectum, bladder, ROP, right femoral head, and left femoral head of VMAT and IMRT plans for the intermediate-risk group

	VMAT		IMRT		*P* value
	Average	±SD	Average	±SD	
PTV					
Mean dose (Gy)	76.00	0.00	76.00	0.00	–
Maximum dose (Gy)	79.40	0.47	78.32	0.60	**0.001**
Minimum dose (Gy)	60.27	2.73	62.92	2.22	**0.037**
CI	0.966	0.012	0.965	0.013	0.937
HI	0.089	0.016	0.083	0.016	0.154
Rectum					
Mean dose (Gy)	28.90	1.89	31.40	2.12	**0.001**
*V*20 (%)	61.38	6.96	69.17	6.40	**< 0.001**
*V*30 (%)	38.77	6.72	45.75	10.00	**0.020**
*V*40 (%)	24.44	3.49	28.91	3.90	**0.003**
*V*50 (%)	16.40	2.43	18.96	2.46	**< 0.001**
*V*60 (%)	10.33	1.58	12.13	1.66	**< 0.001**
*V*70 (%)	4.12	0.68	4.47	0.75	**0.015**
Bladder					
Mean dose (Gy)	26.36	9.61	26.90	9.69	0.216
*V*20 (%)	46.55	18.84	47.93	18.48	0.162
*V*30 (%)	37.65	16.55	39.06	16.48	0.054
*V*40 (%)	28.70	12.98	29.52	12.85	0.135
*V*50 (%)	21.51	9.90	22.61	10.34	**0.011**
*V*60 (%)	16.10	7.57	16.99	8.20	**0.016**
*V*70 (%)	10.06	5.32	11.39	5.94	**0.003**
ROP					
Mean dose (Gy)	70.62	0.95	70.79	0.73	0.237
*V*40 (%)	100.00	0.00	100.00	0.00	–
Right femoral head					
Mean dose (Gy)	14.14	4.65	13.03	4.82	0.148
*V*40 (%)	0.00	0.00	0.00	0.00	–
Left femoral head					
Mean dose (Gy)	15.33	5.16	13.73	4.89	**0.038**
*V*40 (%)	0.00	0.00	0.00	0.00	–

Values in bold are statistically significant

PTV planning target volume, *ROP* rectum overlapped with PTV, *VMAT* volumetric-modulated arc therapy, *IMRT* intensity-modulated radiation therapy, *SD* standard deviation, *CI* conformity index, *HI* homogeneity index, *Vx* percentage volume receiving at least *x* Gy

These results indicate that the VMAT plans provided a dosimetric advantage by sparing the dose to the rectum compared to the IMRT plans. The bladder received a greater average mean dose in the VMAT plans compared to that in the IMRT plans (Table 5). However, the difference between the plans was not statistically significant. The VMAT plans resulted in statistically lower volume percentages received by the bladder at 50, 60, and 70 Gy than those of the IMRT plans (Table 5). Therefore, VMAT could reduce higher dose volumes for the bladder, compared with IMRT.

For the ROP region, the average mean dose was lower in the VMAT compared with the IMRT plans, and the difference was not statistically significant (Table 5). The *V*40 of the ROP region was 100% for both VMAT and IMRT plans (Table 5). For the femoral head, compared with the IMRT plans, average mean doses to femoral heads were greater in the VMAT plans for both the right and left femoral heads (Table 5). The *V*40 of the right and left femoral heads was 0% for both the VMAT and IMRT plans

Table 4 Averages and standard deviations of the dosimetric indices for PTV, rectum, bladder, ROP, right femoral head, and left femoral head of VMAT and IMRT plans for the high-risk group

	VMAT		IMRT		*P* value
	Average	±SD	Average	±SD	
PTV					
Mean dose (Gy)	76.00	0.00	76.00	0.00	–
Maximum dose (Gy)	79.20	0.48	78.35	0.80	**< 0.001**
Minimum dose (Gy)	62.11	1.89	62.87	2.73	0.329
CI	0.959	0.017	0.967	0.015	0.187
HI	0.091	0.019	0.081	0.018	0.050
Rectum					
Mean dose (Gy)	27.63	3.26	29.91	3.51	**< 0.001**
*V*20 (%)	57.29	9.63	62.62	9.88	**0.007**
*V*30 (%)	36.73	8.09	42.63	7.82	**< 0.001**
*V*40 (%)	24.26	4.59	28.45	5.09	**< 0.001**
*V*50 (%)	16.53	2.98	20.65	4.98	**0.002**
*V*60 (%)	10.45	1.95	14.47	6.13	**0.039**
*V*70 (%)	4.19	1.02	6.64	5.67	0.174
Bladder					
Mean dose (Gy)	27.24	9.97	25.55	10.24	0.261
*V*20 (%)	48.90	19.80	46.08	19.45	0.343
*V*30 (%)	38.19	19.84	36.05	18.86	0.445
*V*40 (%)	28.65	16.36	27.05	15.63	0.429
*V*50 (%)	20.21	11.47	20.96	12.46	0.860
*V*60 (%)	15.55	8.08	15.64	9.09	0.929
*V*70 (%)	10.02	5.23	10.43	5.94	**0.009**
ROP					
Mean dose (Gy)	70.44	0.62	70.92	1.27	0.219
*V*40 (%)	100.00	0.00	100.00	0.00	
Right femoral head					
Mean dose (Gy)	12.57	4.44	12.00	4.52	0.418
*V*40 (%)	0.00	0.00	0.00	0.00	
Left femoral head					
Mean dose (Gy)	14.03	5.24	12.46	12.46	0.014
*V*40 (%)	0.00	0.00	0.00	0.00	

Values in bold are statistically significant

PTV planning target volume, *ROP* rectum overlapped with PTV, *VMAT* volumetric-modulated arc therapy, *IMRT* intensity-modulated radiation therapy, *SD* standard deviation, *CI* conformity index, *HI* homogeneity index, *Vx* percentage volume receiving at least *x* Gy

Table 5 Averages and standard deviations of the dosimetric indices for PTV, rectum, bladder, ROP, right femoral head, and left femoral head of VMAT and IMRT plans for all-risk groups

	VMAT		IMRT		*P* value
	Average	±SD	Average	±SD	
PTV					
Mean dose (Gy)	76.00	0.00	76.00	0.00	–
Maximum dose (Gy)	79.36	0.53	78.28	0.61	**< 0.001**
Minimum dose (Gy)	61.28	2.38	62.68	2.39	**0.007**
CI	0.963	0.014	0.954	0.014	**0.046**
HI	0.094	0.019	0.086	0.019	**0.010**
Rectum					
Mean dose (Gy)	27.81	2.75	29.96	2.96	**< 0.001**
*V*20 (%)	57.59	7.85	63.67	8.47	**< 0.001**
*V*30 (%)	36.86	7.02	42.54	8.01	**< 0.001**
*V*40 (%)	24.05	4.44	27.72	4.73	**< 0.001**
*V*50 (%)	16.27	3.04	19.12	4.07	**< 0.001**
*V*60 (%)	10.29	1.98	12.71	4.22	**< 0.001**
*V*70 (%)	4.05	0.97	4.95	3.66	0.130
Bladder					
Mean dose (Gy)	26.67	9.97	26.52	10.10	0.511
*V*20 (%)	47.14	19.73	47.66	18.32	**0.017**
*V*30 (%)	37.97	18.59	38.30	18.32	0.701
*V*40 (%)	28.74	14.90	28.79	14.64	0.950
*V*50 (%)	21.44	11.39	22.04	11.39	**0.019**
*V*60 (%)	15.94	8.45	16.41	8.45	**0.001**
*V*70 (%)	10.09	5.61	10.85	5.61	**< 0.001**
ROP					
Mean dose (Gy)	70.34	0.88	70.58	1.14	0.115
*V*40 (%)	100.00	0.00	100.00	0.00	–
Right femoral head					
Mean dose (Gy)	13.70	4.20	12.79	4.18	**0.038**
*V*40 (%)	0.00	0.00	0.00	0.00	–
Left femoral head					
Mean dose (Gy)	14.92	4.20	13.19	4.33	**< 0.001**
*V*40 (%)	0.00	0.00	0.00	0.00	–

Values in bold are statistically significant

PTV planning target volume, *ROP* rectum overlapped with PTV, *VMAT* volumetric-modulated arc therapy, *IMRT* intensity-modulated radiation therapy, *SD* standard deviation, *CI* conformity index, *HI* homogeneity index, *Vx* percentage volume receiving at least *x* Gy

(Table 5). These results indicated that IMRT produced better dose-sparing of the femoral heads than VMAT.

Figure 4a shows the average numbers of cold spots per PTV of the three risk groups for the VMAT and IMRT plans. The error bars indicate the standard deviations. The averages ± standard deviations of the numbers of cold spots per PTV of all-risk groups for the VMAT and IMRT plans were 0.21 ± 0.10 cm^{-3} and 0.24 ± 0.08 cm^{-3}, respectively ($P = 0.158$). There was no significant difference between the VMAT and IMRT plans for the average numbers of cold spots per PTV for each type of risk. Figure 4b shows the average volume percentages of cold spots in the PTV of the three risk groups in the VMAT and IMRT plans. The average volume percentage of cold spots per PTV for all risks was $4.37 \pm 2.68\%$ for the VMAT, which was smaller than the $5.72 \pm 1.84\%$ observed for the IMRT plans ($P = 0.007$). As for the high-risk group, the average volume percentage of cold spots for VMAT was statistically smaller than that for IMRT plans ($P < 0.001$).

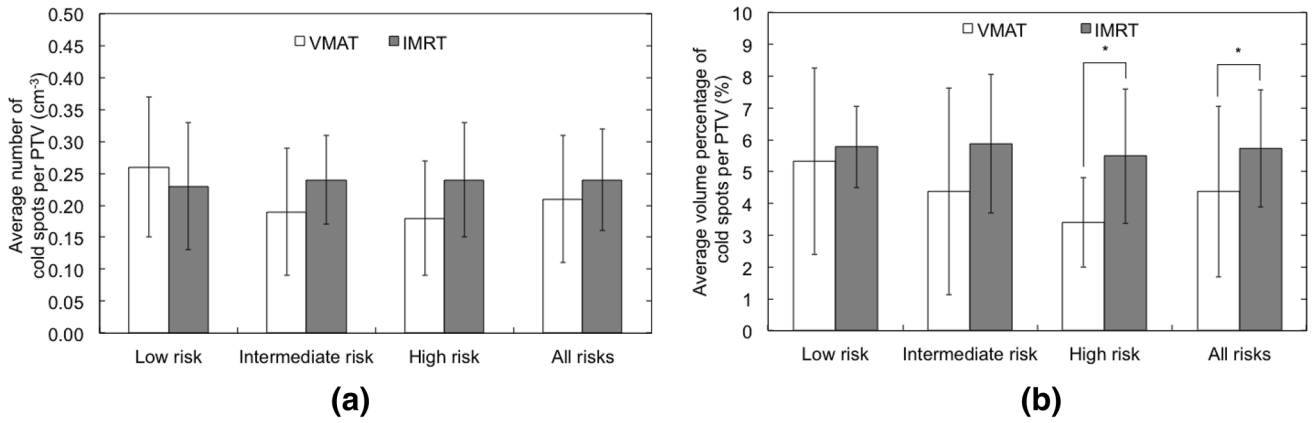

Fig. 4 **a** Average numbers and **b** volume percentages of cold spots per PTV of three risk groups for VMAT and IMRT plans. The error bars and asterisks indicate the standard deviations and statistically significant differences ($P < 0.05$), respectively

Figure 5a, b shows the average numbers and volume percentages of cold spots per ROP region of the three risk groups for the VMAT and IMRT plans, respectively. The average of cold spots per ROP region of all-risk groups for VMAT number (0.99 ± 0.85 cm^{-3}) did not significantly differ from that (0.96 ± 0.94 cm^{-3}) for IMRT plans ($P = 0.827$), as shown in Fig. 5a. Additionally, the average volume percentage ($70.61 \pm 14.77\%$) of cold spots per ROP region for the VMAT did not significantly differ from that ($65.07 \pm 19.3\%$) for the IMRT plans ($P = 0.087$), as shown in Fig. 5b. There was no significant difference between the VMAT and IMRT plans regarding the average number and volume percentage of cold spots per ROP region for each type of risk.

Figure 6 shows the 3D PDs of the probability and distributions of cold spots in the VMAT and IMRT plans for the low-risk group, the intermediate-risk group, the high-risk group, and all-risk groups. The logical OR region of the PTVs is shown in light green, while the PD of the probability and distributions of cold spots is shown in red with opacity. Figure 6a–d shows that the cold spots are widely distributed throughout PTVs in both VMAT and IMRT plans. However, in the anterior–posterior (AP) and left–right (LR) views, most of the cold spots are distributed on the posterior and upper PTVs for both plans. In addition, the 3D PDs of the probability and distributions of cold spots in the ROP regions in the VMAT and IMRT plans for low-risk group, intermediate-risk group, high-risk group, and all-risk groups are shown in Fig. 7a–d.

Table 6 shows volumes of cold-spot-existence-probability distributions more than several probabilities for VMAT and IMRT plans. The probabilistic volumes of cold spots were estimated at different distribution probabilities of cold spots for VMAT and IMRT plans. The volume (3.86 cm^3) more than a distribution probability of 0.3 of cold spots for VMAT was smaller than that (5.10 cm^3) for IMRT plans. These probabilistic volumes of cold spots indicate that the probability of the existence of cold spots in VMAT is smaller than IMRT plans. However, at low

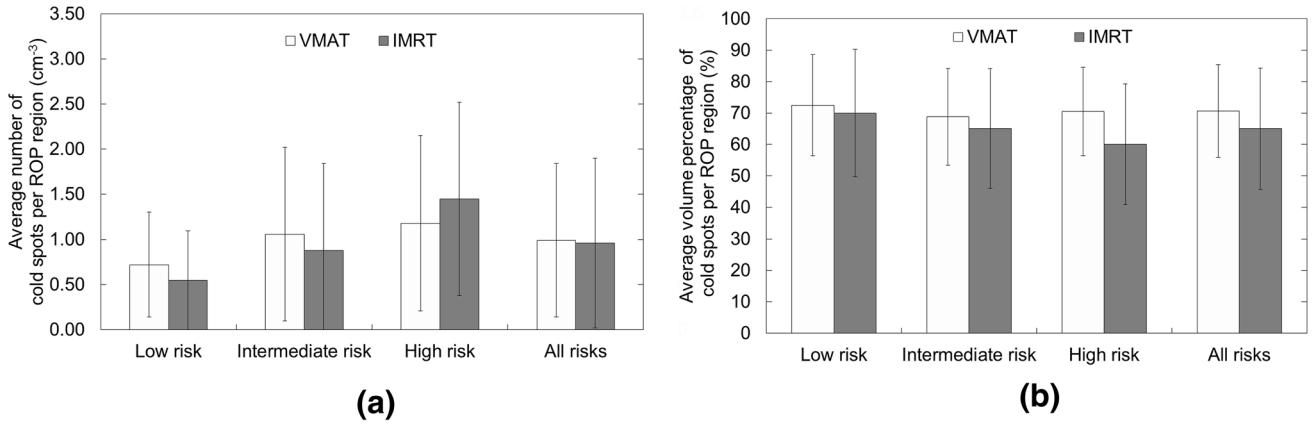

Fig. 5 **a** Average numbers and **b** volume percentages of cold spots per ROP region of three risk groups for VMAT and IMRT plans. The error bars indicate the standard deviations

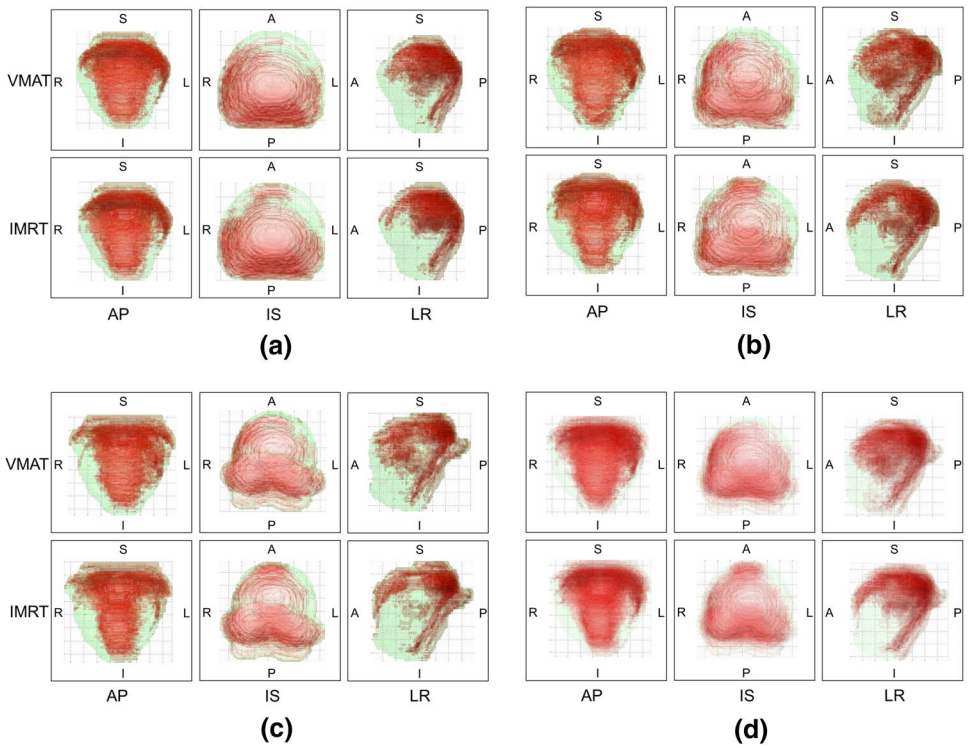

Fig. 6 Three-dimensional probabilistic distributions of the probability and distributions of cold spots in VMAT and IMRT plans in anterior–posterior (AP), inferior–superior (IS), and left–right (LR) views for **a** low-risk group, **b** intermediate-risk group, **c** high-risk group, and **d** all-risk groups

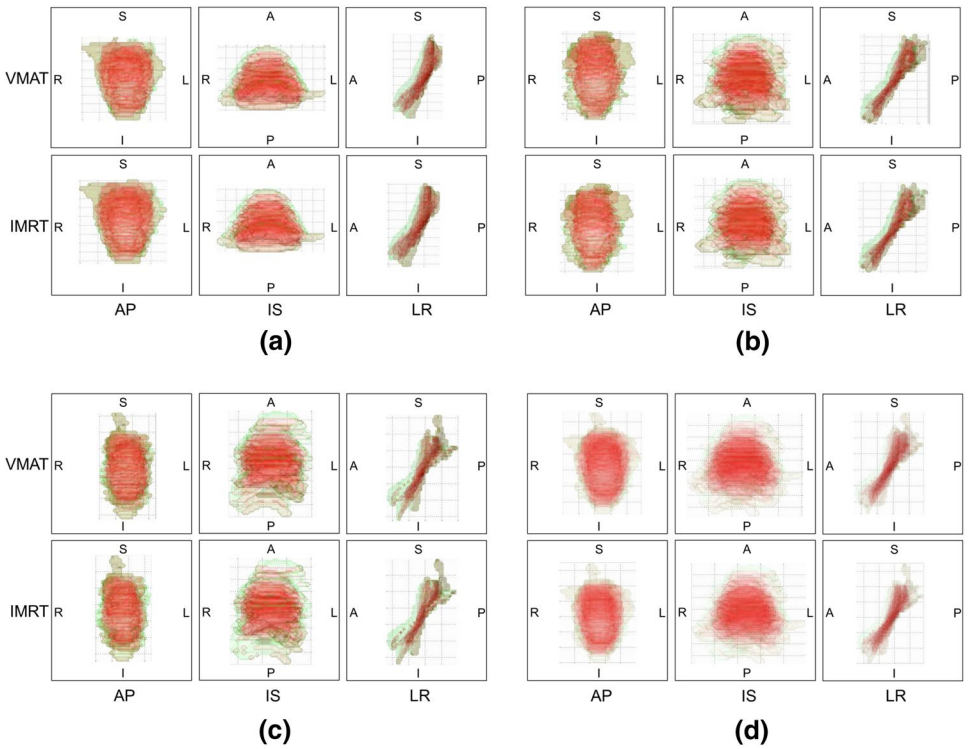

Fig. 7 Three-dimensional probabilistic distributions of the probability and distributions of cold spots in ROP regions in VMAT and IMRT plans in anterior–posterior (AP), inferior–superior (IS), and left–right (LR) views for **a** low-risk group, **b** intermediate-risk group, **c** high-risk group, and **d** all-risk groups

probabilities of cold spots (0.1), the volume of cold spots for VMAT (239.08 cm^3) was larger than that for IMRT plans (235.91 cm^3). This is because the cold spots in VMAT are more widely distributed than those of IMRT plans, as shown in Fig. 6a–d.

4 Discussion

This study compared the dosimetric qualities of VMAT and IMRT plans using dosimetric indices and analyzed

Table 6 Volumes of cold-spot-existence-probability distributions for several probabilities in VMAT and IMRT plans

Probability for threshold	Probabilistic volume of cold spots (cm^3)	
	VMAT	IMRT
0	1019.24	1019.14
0.1	239.08	235.91
0.2	44.35	44.51
0.3	3.86	5.10
0.4	0.03	0.11

VMAT volumetric-modulated arc therapy, *IMRT* intensity-modulated radiation therapy

cold spots in prostate cancer. The VMAT provided dosimetric advantages over the IMRT plans with respect to target dose conformity, dose-sparing of the rectum and bladder (Table 5), and cold spots (Fig. 4b; Table 6), but achieved worse target dose homogeneity and dose-sparing of the right and left femoral heads compared to those of the IMRT plans (Table 5).

Previous studies have reported similar results for target dose conformity and OAR dose-sparing in dosimetric comparisons for the treatment of prostate cancer [16–20, 22, 24]. However, some dosimetric comparison results in the present study differed from those reported other studies [21, 23, 25]. Yoo et al. showed a better dose conformity in the PTV but worse rectum and bladder dose-sparing by VMAT compared to those in IMRT plans [21]. Differences in VMAT and IMRT techniques, plan objectives, beam angles, etc., may have contributed to this difference in results. Another factor may be related to differences in the volume and shape of the PTV due to different CTV definitions at different institutes and differences in patient risk groups. All of these factors might affect the dosimetric outcomes.

Divergent delineation policies for the three risk groups in prostate cancer cases may lead to differences in the results of VMAT and IMRT plans. There were some differences in the results among risk groups, for example, results for PTV and femoral head in Table 5 (summary of all-risk groups) were partially different from those in Table 2 (low-risk group), Table 3 (intermediate-risk group), and Table 4 (high-risk group). For instance, there were no statistically significant differences in average minimum doses to PTV between VMAT and IMRT plans in low- and high-risk groups (Tables 2, 4), whereas average minimum doses in VMAT plans were significantly lower than those in IMRT plans, with respect to intermediate-risk and all-risk groups (Tables 3, 5). In addition, there were no statistically significant differences in the CI and HI between VMAT and IMRT plans among the three risk groups (Tables 2, 3, 4); however, there were statistically significant differences in those parameters when all-risk groups were analyzed together (Table 5). Furthermore, the delineation policy of three risk groups in prostate cancer cases could have an impact on the results pertaining to the femoral head. In the intermediate-risk and all-risk groups (Tables 3, 5), the average mean doses to left femoral heads in VMAT plans were significantly greater than those in IMRT plans. Additionally, only analyzing all-risk groups together (Table 5) showed that the mean dose to the right femoral heads was significantly greater in VMAT compared with IMRT plans.

The difference of optimization algorithms between VMAT (PRO algorithm) and IMRT (DVO algorithm) may affect the dosimetric results of VMAT and IMRT plans. While a simple gradient method was employed for the IMRT plans, a simulated annealing method was employed for the VMAT plans. In the latter, one of the variables in the simulated annealing is randomly selected and its value is randomly increased or decreased by a small amount [38]. This could result in better optimization results and may achieve better plans, because trapping in the local minimum is avoided [39]. For example, the effect of difference in optimization algorithms is shown in Fig. 4b for the high-risk group. In addition, we think that VMAT could reduce cold spot occurrence by irradiation from many gantry angles and delivery times optimized in that algorithm.

Because cold spots in the PTV could induce tumor recurrence, we also analyzed the numbers, volumes, and distributions of cold spots between the VMAT and IMRT plans. Figure 4a, b indicates that VMAT plans result in cold spots with smaller volumes in the PTV than those in the IMRT plans, as shown by the probability of 0.3 of cold spots in Table 6, whereas the cold spots in the VMAT were distributed more widely than those in the IMRT plans, as shown in Fig. 6a–d. The reason for this phenomenon is that the VMAT can irradiate from more directions than IMRT, which averages the VMAT irradiation to a rotating target, whereas IMRT irradiates from only seven directions. Figure 6a–d shows the distributions of cold spots on the posterior and upper PTVs for all types of risk groups in the VMAT and IMRT plans. The reason for this distribution is that the ROP region is not regarded as a target for dose calculation in planning the radiotherapy of prostate cancer to avoid high irradiating doses to the rectum (OAR) [40, 41]. Therefore, cold spots were distributed throughout nearly all of parts of the ROP regions (Fig. 7a–d), as also evidenced by the volume percentages of cold spots per ROP for the VMAT and IMRT plans in Fig. 5b. Considering the differences in the distributions of cold spots between the VMAT and IMRT plans, the volumes of cold spots in the VMAT was smaller than those of the IMRT (Fig. 4b), whereas there was no significant difference in the volume of cold spots in the ROP regions between the plans (Fig. 5b). These results indicated that the volume of

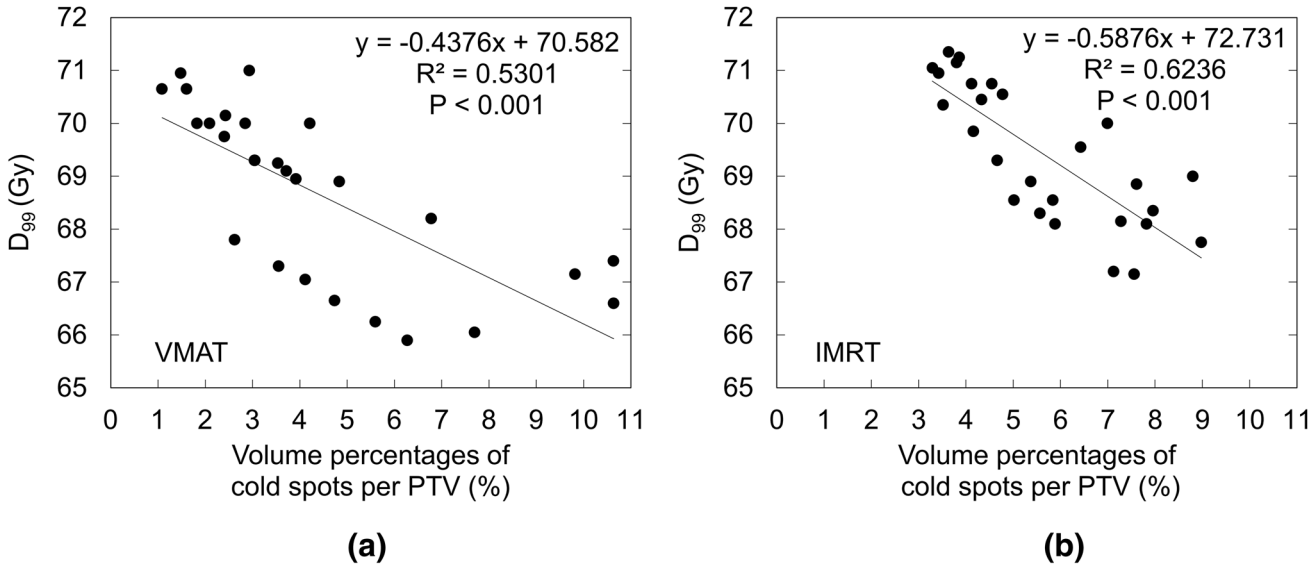

Fig. 8 Relationship between volume percentages of cold spots per PTV and D_{99} for **a** VMAT and **b** IMRT plans

cold spots in other parts of the PTV (except for the ROP regions) in VMAT was smaller than that of the IMRT plans.

To understand how much the cold spot occurrence affects DVH, we investigated the relationship between the volume percentage of cold spots per PTV (%) and D_{99} (Gy) for (a) VMAT and (b) IMRT plans, as shown in Fig. 8. Figure 8 indicates that D_{99} representing the minimum dose delivered to 99% of the PTV decreased with increasing of the volume of cold spots for both VMAT and IMRT plans. The average ± SD of D_{99} for VMAT plans was 68.68 ± 2.63 Gy, which was smaller than 69.42 ± 1.73 Gy for IMRT plans ($P = 0.002$). In other words, there are negative correlations between the cold spot volume per PTV and D_{99} for VMAT and IMRT plans. This result does not correspond that the average volume percentage of cold spots per PTV for the VMAT plans was 4.37 ± 2.68%, which was smaller than the 5.72 ± 1.84% observed for IMRT plans ($P = 0.007$). Consequently, the cold spots would not affect the DVH at least D_{99}.

This study had three limitations. First, we used the definition of cold spots based on the use of the trial guidelines of the RTOG H-0222 in head and neck cancers. Second, many cold spots were distributed on the upper PTVs, as shown in Fig. 6a–d. Further consideration is needed to assess the distributions of these cold spots in VMAT and IMRT plans. Third, 30 patients with only ten cases for each risk group were selected for this study. Therefore, data from a larger number of cancer patients in each risk group are required to improve the accuracy of the prediction of the PD of cold spots.

5 Conclusions

This study compared the dosimetric indices and analyzed the numbers, volume percentages, and PD of the probability and distributions of cold spots for VMAT and IMRT prostate cancer plans. VMAT plans achieved better target dose conformity, OAR (rectum, bladder) dose-sparing, and smaller cold spots than those of the IMRT plans in the radiation treatment of prostate cancer.

Acknowledgements Funding was provided by Japan Society for the Promotion of Science (Grant no: 16J04075).

Compliance with ethical standards

Conflict of interest The authors declare that they have no conflict of interest.

Statements of human rights All procedures performed in studies involving human participants were in accordance with the ethical standards of the Institutional Review Board (IRB) and with the 1964 Declaration of Helsinki and its later amendments or comparable ethical standards.

Statements of animal rights This article does not contain any studies using animals.

Informed consent Informed consent was obtained from all individual participants included in the study.

References

1. Ferlay J, Soerfomataram I, Dikshit R, et al. Cancer incidence and mortality worldwide: sources, methods and major patterns in GLOBOCAN 2012. Int J Cancer. 2015;136:359–86.

2. Kitazawa T, Matsumoto K, Fujita S, et al. Cost of illness of the prostate cancer in Japan—a time-trend analysis and future projections. BMC Health Serv Res. 2015;15:453.
3. Ogawa K, Nakamura K, Sasaki T, et al. Radical external beam radiotherapy for clinically localized prostate cancer in Japan: changing trends in the patterns of care process survey. Int J Radiat Oncol Biol Phys. 2011;81:1310–8.
4. King CR, Dipetrillo TA, Wazer DE, et al. Optimal radiotherapy for prostate cancer: predictions for conventional external beam, IMRT, and brachytherapy from radiobiologic models. Int J Radiat Oncol Biol Phys. 2000;46:165–72.
5. Ezzell GA, Galvin JM, Low D, et al. Guidance document on delivery, treatment planning, and clinical implementation of IMRT: report of the IMRT Subcommittee of the AAPM Radiation Therapy Committee. Med Phys. 2003;30:2089–115.
6. Hodapp N. The ICRU Report 83: prescribing, recording and reporting photon-beam intensity-modulated radiation therapy (IMRT). Strahlenther Onkol. 2012;188:97–9.
7. Rana S. Intensity modulated radiation therapy versus volumetric intensity modulated arc therapy. J Med Radiat Sci. 2013;60:81–3.
8. Otto K. Volumetric modulated arc therapy: IMRT in a single gantry arc. Med Phys. 2008;35:310–7.
9. Jeraj R, Keall PJ, Siebers JV. The effect of dose calculation accuracy on inverse treatment planning. Phys Med Biol. 2002;47:391–407.
10. Mundt AJ, Roeske JC. Intensity modulated radiation therapy: a clinical perspective. Hamilton: BC Decker Inc.; 2005.
11. Dogan N, Siebers JV, Keall PJ, et al. Improving IMRT dose accuracy via deliverable Monte Carlo optimization for the treatment of head and neck cancer patients. Med Phys. 2006;33:4033–43.
12. Bortfeld T, Craft D, Dempsey JF, et al. Evaluating target cold spots by the use of tail EUDs. Int J Radiat Oncol Biol Phys. 2008;71:880–9.
13. Tomé WA, Fowler JF. On cold spots in tumor subvolumes. Med Phys. 2002;29:1590–8.
14. Vora SA, Wong WW, Schild SE, et al. Outcome and toxicity for patients treated with intensity modulated radiation therapy for localized prostate cancer. J Urol. 2013;190:521–6.
15. Zaorsky NG, Shaikh T, Murphy CT, et al. Comparison of outcomes and toxicities among radiation therapy treatment options for prostate cancer. Cancer Treat Rev. 2016;48:50–60.
16. Palma D, Vollans E, James K, et al. Volumetric modulated arc therapy for delivery of prostate radiotherapy: comparison with intensity-modulated radiotherapy and three-dimensional conformal radiotherapy. Int J Radiat Oncol Biol Phys. 2008;72:993–1001.
17. Wolff D, Stieler F, Welzel G, et al. Volumetric modulated arc therapy (VMAT) vs. serial tomotherapy, step-and-shoot IMRT and 3D-conformal RT for treatment of prostate cancer. Radiother Oncol. 2009;93:226–33.
18. Quan EM, Li X, Li Y, et al. A comprehensive comparison of IMRT and VMAT plan quality for prostate cancer treatment. Int J Radiat Oncol Biol Phys. 2012;83:1169–78.
19. Guckenberger M, Richter A, Krieger T, et al. Is a single arc sufficient in volumetric-modulated arc therapy (VMAT) for complex-shaped target volumes? Radiother Oncol. 2009;93:259–65.
20. Kjaer-Kristofferesen F, Ohlhues L, Medin J, et al. RapidArc volumetric modulated therapy planning for prostate cancer patients. Acta Oncol. 2009;48:227–32.
21. Yoo S, Wu QJ, Lee WR, et al. Radiotherapy treatment plans with RapidArc for prostate cancer involving seminal vesicles and lymph nodes. Int J Radiat Oncol Biol Phys. 2009;76:935–42.
22. Ost P, Speleers B, De Meerleer G, et al. Volumetric arc therapy and intensity modulated radiotherapy for primary prostate radiotherapy with simultaneous integrated boost to intraprostatic lesion with 6 and 18 MV: A planning comparison study. Int J Radiat Oncol Biol Phys. 2011;79:920–6.
23. Sze HC, Lee MC, Hung WM, et al. RapidArc radiotherapy planning for prostate cancer: single-arc and double-arc techniques vs. intensity modulated radiotherapy. Med Dosim. 2012;37:87–91.
24. Shaffer R, Morris WJ, Moiseenko V, et al. Volumetric modulated arc therapy and conventional intensity-modulated radiotherapy for simultaneous maximal intraprostatic boost: a planning comparison study. Clin Oncol R Coll Radiol. 2009;21:401–7.
25. Kopp RW, Duff M, Catalfamo F, et al. VMAT vs. 7-field-IMRT: assessing the dosimetric parameters of prostate cancer treatment with a 292-patient sample. Med Dosim. 2011;36:365–72.
26. Haekal M, Arimura H, Hirose T, et al. Computational analysis of interfractional anisotropic shape variations of the rectum in prostate cancer radiation therapy. Phys Medica. 2018;46:168–79.
27. Boehmer D, Maingon P, Poortmans P, et al. Guidelines for primary radiotherapy of patients with prostate cancer. Radiother Oncol. 2006;79:259–69.
28. Hayden AJ, Martin JM, Kneebone AB, et al. Australian and New Zealand faculty of radiation oncology genito-urinary group: 2010 consensus guidelines for definitive external beam radiotherapy for prostate carcinoma. J Med Imaging Radiat Oncol. 2010;54:513–25.
29. Bragg C, Windate K, Conway J. Clinical implications of the anisotropic analytical algorithm for IMRT treatment planning and verification. Radiother Oncol. 2008;86:276–84.
30. Michalski J. Purdy J, Bruner DW, et al., Radiation Therapy Oncology Group (RTOG) Report No. 0126, 2004.
31. Parker J, Kenyon R, Troxel D. Comparison of interpolating methods for image resampling. IEEE Trans Med Imag. 1983;2:31–9.
32. International Commission on Radiation Units and Measurements. ICRU Report 62. Prescribing, Recording, and Reporting Photon Beam Therapy (Supplement to ICRU Report 50). J ICRU. 1999.
33. Paddick I. A simple scoring ratio to index the conformity of radiosurgical treatment plans. Technical note. J Neurosurg. 2000;93:219–22.
34. Feuvret L, Noel G, Mazeron JJ, et al. Conformity index: a review. Int J Radiat Oncol Biol Phys. 2006;64:333–42.
35. Shapiro LG. Connected component labeling and adjacency graph con-struction. Mach Intell Pattern Recognit. 1996;19:1–30.
36. Lumia RA. New three-dimensional connected components algorithm. Compt Vis Graph Image Process. 1983;22:207–20.
37. Shibayama Y, Arimura H, Hirose TA, et al. Investigation of interfractional shape variations based on statistical point distribution model for prostate cancer radiation therapy. Med Phys. 2017;44:1837–45.
38. Taqaddas AE. Investigation of VMAT algorithms and dosimetry. London: AuthorHouse UK Publishing; 2011.
39. Khan M. Treatment planning in radiation oncology. Philadelphia: Lippincott Williams and Wilkins; 2007.
40. McLaughlin PW, Wygoda A, Sahijdak W, et al. The effect of patient position and treatment technique in conformal treatment of prostate cancer. Int J Radiat Oncol Biol Phys. 1999;45:407–13.
41. Serrano NA, Kalman NS, Anscher MS. Reducing rectal injury in men receiving prostate cancer radiation therapy: current perspectives. Cancer Manag Res. 2017;9:339–50.